Internal Motions of both Poly(*N*-isopropylacrylamide) Linear Chains and Spherical Microgel Particles in Water

Chi Wu* and Shuiqin Zhou

Department of Chemistry, The Chinese University of Hong Kong, Shatin, N.T., Hong Kong

Received May 18, 1995; Revised Manuscript Received June 22, 1995[⊗]

ABSTRACT: Poly(*N*-isopropylacrylamide) (PNIPAM) linear chains and spherical microgel particles in very dilute aqueous solutions were studied by dynamic laser light scattering (LLS) over a wide range of scattering angles (6−154°). For the linear chains, at $x < 1$, only one peak related to diffusion was observed in the line-width distribution $G(\Gamma)$, while for $x > 1$, we detected a second peak related to internal motions, where $x = (qR_g)^2$ with q and R_g the scattering vector and the radius of gyration, respectively. The average line width of the second peak can be related to some internal motions predicted in the nondraining bead-and-spring model, but other predicted internal motions are not observable. In the swollen microgel particles ($R_g \sim 160$ nm), the internal motions were only observed at $x \geq 13$ ($1/q \geq 44$ nm). At very high x, in both the chains and particles, the two peaks merge into one broad peak and the plot of $\langle\Gamma\rangle/q^3$ vs $x^{1/2}$ approaches two different plateaus, where $\langle\Gamma\rangle = \int_0^\infty G(\Gamma)\Gamma\, d\Gamma$. Both of the plateaus are lower than predicted in the bead-and-spring model. The plateau of the particles is much lower than that of the chains. Energetically favorable internal motions may not be observable in dynamic LLS, possibly due to the observation length scale ($1/q$).

Introduction

The dynamics of flexible polymer chains in dilute solution is a fundamental problem in polymer physics, which has long been theoretically investigated and experimentally examined.[1−6] The relaxation processes associated with internal motions of flexible polymer chains in dilute solution will add additional broadening to the spectral distribution of the scattered light.[7] Quantitative predictions of this spectral broadening have been made on the basis of various modified bead-and-spring models with (or without) consideration of hydrodynamic interactions.[8,9] However, these theories are not very successful in describing the measured spectral distributions at x [$\equiv(qR_g)^2$] > 3, where R_g ($=\langle R_g^2\rangle_z^{1/2}$) is the root-mean-square z-average radius of gyration and $q = (4\pi n/\lambda_0)\sin(\theta/2)$ is the scattering vector with n, λ_0, and θ being the solvent refractive index, the wavelength in vacuo, and scattering angle, respectively.

The study of internal motions in dilute solution has been an experimental challenge for years. In order to see as many internal modes as possible, narrowly distributed, long (high molecular mass), flexible polymer chains have to be used. For such polymer chains, there always exists a certain degree of coupling between the translational diffusion and the internal motions at the typical accessible small scattering angle (∼15°) of a normal dynamic laser light scattering (LLS) spectrometer. A clear separation of these two types of motions is vital for a reliable investigation of internal motions. Recently, both Chu *et al.*[10] and Wu *et al.*[11] have studied the internal motions of high molecular weight polystyrenes in dilute toluene solutions by combining the line-width distributions $G(\Gamma)$ measured at very small scattering angles (<6° in two specially designed LLS spectrometers) with those measured at high angles. Several high-order internal motions were observed. Wu *et al.*[11] noted that some energetically favored internal motions predicted in the bead-and-spring model were missed in dynamic LLS. Moreover, Wu *et al.*[11] noted that the plateau in the plot of $\langle\Gamma\rangle/(q^3k_BT/\eta_0)$ vs $x^{1/2}$ is lower than predicted in the bead-and-spring model, where $\langle\Gamma\rangle$, k_B, T, and η_0 are the overall average line width, the Boltzmann constant, the absolute temperature, and the solvent viscosity, respectively. This lower plateau value also implies that some predicted internal motions are not observable in dynamic LLS. These contradictions between the prediction and experimental data led us to speculate that the missing of some predicted internal motions in dynamic LLS is related to the observation length scale $1/q$.

In this study, a water-soluble, narrowly distributed, high molecular weight polymer, poly(*N*-isopropylacrylamide) (PNIPAM), was chosen to find how different polymer/solvent and polymer segment/segment interactions affect the dynamics of flexible polymer chains in very dilute solutions. If the observed lower plateau at larger x is due to the missing of some predicted internal motions, we should observe an even lower plateau in the plot of $\langle\Gamma\rangle/(q^3k_BT/\eta_0)$ vs $x^{1/2}$ for a cross-linked polymer network where the internal motions have been greatly suppressed. Therefore, the dynamics of very narrowly distributed spherical PNIPAM microgel particles ($R_g \sim$ 160 nm) in very dilute solutions were also studied by dynamic LLS over a wide range of the scattering angle, especially at larger scattering angles.

Theoretical Background

Pecora showed that when an infinitely dilute polymer solution is illuminated by a coherent and monochromatic laser light beam, the spectral distribution of the light scattered from a flexible polymer chain can be written as[12]

$$S(q,\omega) = (1/2\pi)\int e^{-i\omega t}e^{-q^2D|t|}J(q,t)\,dt \qquad (1)$$

where ω is the difference between the angular frequency of the scattered and the incident light, q is the scattering vector as previously defined, D is the translational diffusion coefficient of the polymer chain, and the function

$$J(q,t) = \langle(1/N^2)\sum_{l=0}^{N}\sum_{m=0}^{N} e^{-i\mathbf{q}\cdot[\mathbf{r}_l(0)-\mathbf{r}_m(t)]}\rangle \qquad (2)$$

[⊗] Abstract published in *Advance ACS Abstracts,* January 1, 1996.

0024-9297/96/2229-1574$12.00/0

Table 1. Laser Light-Scattering Results of Individual PNIPAM Linear Chains and Microgel Particles in Very Dilute Aqueous Solutions at $T = 15$ °C[a]

PNIPAM sample	M_w (10^7 g/mol)	R_g (nm)	M_w/M_n	D (μm^2/s)	R_h (nm)	R_g/R_h
single chain	1.21	180	~1.05	1.61	116	1.55
microgel	22.0	160	~1.05	0.98	190	0.84

[a] Relative errors: M_w, ±3%; R_g, ±5%; D and R_h, ±1%.

is the spatial Fourier transform of the segment−segment time correlation function. It arises from the interference of the scattered light from different segments in the polymer chain containing N such segments. $J(q,t)$ contains all the temporal and spatial information on the intramolecular (or internal) motion of the polymer chain. $\mathbf{r}_l(0)$ is the position of the lth segment at time 0, and $\mathbf{r}_m(t)$ is the position of the mth segment at time t, both referred to the center of mass of the polymer.

In order to perform the ensemble average in $J(q,t)$, a model for the internal motion of a chain is needed. By incorporating the Oseen−Kirkwood−Riseman hydrodynamic interaction into the bead-and-spring model, Perico, Piaggio, and Cuniberti (PPC) have shown[13] that

$$S(q,\omega) = P_0(x)L(\omega,q^2D) + \sum_{\alpha=1}^{N} P_1(x,\alpha)L(\omega,q^2D+\Gamma_\alpha) + \sum_{\alpha=1}^{N}\sum_{\beta=1}^{N} P_2(x,\alpha,\beta)L(\omega,q^2D+\Gamma_\alpha+\Gamma_\beta) + \sum_{\alpha=1}^{N}\sum_{\beta=1}^{N}\sum_{\gamma=1}^{N} P_3(x,\alpha,\beta,\gamma)L(\omega,q^2D+\Gamma_\alpha+\Gamma_\beta+\Gamma_\gamma) + \ldots \quad (3)$$

where the functions

$$L(\omega,\Gamma) = \frac{2\Gamma}{2\pi(\omega^2+\Gamma^2)} \quad (4)$$

represent the ω-normalized Lorentzian distributions with Γ the half-width at half-height, i.e., the line width, and the P_n ($n = 0, 1, \ldots$) determines the contribution of each Lorentzian to the spectrum $G(\Gamma)$ of the scattered light. The zeroth-order $P_0(x)$ represents the contribution from the translational diffusion; $P_1(x,\alpha)$, the first-order contribution of the αth internal mode; $P_2(x,\alpha,\beta)$, the second-order contribution of the αth and βth internal modes; and so on. When $x < 1$, the spectral distribution is measured in the long-wavelength regime and the polymer chain is viewed as a point. Hence, $P_0(x)$ is dominant in $S(q,\omega)$. As x increases, the light probes a portion of the chains and the contributions from $P_1(x,\alpha)$, $P_2(x,\alpha,\beta)$, and other higher order terms become more and more important. PPC have numerically shown that $P_2(x,1,1)$ is the largest contribution to $S(q,\omega)$ among all Lorentzian terms associated with the internal modes.[13]

In a modern dynamic laser light scattering experiment, the intensity−intensity time correlation function of the scattered light can be measured, from which $S(q,t)$, the Fourier transform of $S(q,\omega)$, is determined.

Experimental Section

Sample Preparation. The high molecular weight and narrowly distributed poly(*N*-isopropylacrylamide) (PNIPAM) was prepared by a fractionation/filtration method.[14,15] The narrowly distributed PNIPAM microgel particles were made by emulsion polymerization. The details have been given before.[16] Table 1 summarizes the weight-average molecular (or particle) mass M_w and the radius of gyration R_g of both the linear PNIPAM chains and spherical microgel particles. In dynamic LLS, the polymer and particle concentrations were so dilute (~1 μg/mL) that the concentration correction on the measured $G(\Gamma)$ was unnecessary (<2% estimated on the basis of the known value of the second virial coefficient A_2). Filters (0.5 μm; Millipore) were used to remove the dust in the solutions. The details of the clarification of the solutions for dynamic LLS were described before.[16]

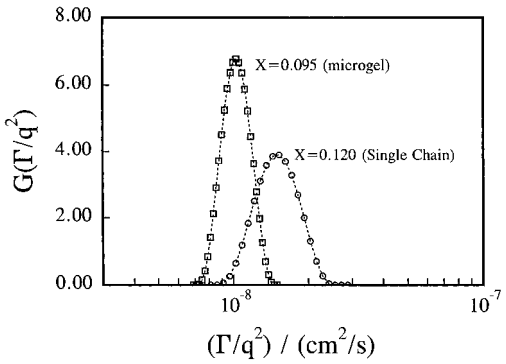

Figure 1. Typical plots of the line-width distributions $G(\Gamma/q^2)$ at $T = 15.0$ °C and $\theta = 7°$.

Dynamic LLS. The intensity−intensity time correlation function $G^{(2)}(t,\theta)$ in the self-beating mode was measured, which has the following form:[17,18]

$$G^{(2)}(q,t) = A[1 + \beta|g^{(1)}(q,t)|^2] \quad (5)$$

where A is a measured baseline; β, a spatial coherence constant depending only on the detection optics (its value $0 \le \beta \le 1$) reflects the signal-to-noise ratio of the actual experiment); and $g^{(1)}(q,t)$, the normalized electric field−field time correlation function. It can be shown that $g^{(1)}(q,t)$ is proportional to the dynamic structure factor $S(q,t)$ and $g^{(1)}(q,t)$ can be related to the characteristic line-width distribution $G(\Gamma)$ by[18]

$$g^{(1)}(q,t) = \int_0^\infty G(\Gamma)e^{-\Gamma t}\,d\Gamma \quad (6)$$

A Laplace inversion of eq 6 gives $G(\Gamma)$ and the inversion can be accomplished by using a CONTIN algorithm.[19] If the relaxation is diffusive, such as for a narrowly distributed polymer sample in dilute solutions at $x \ll 1$, $G(\Gamma)$ is related to a translational diffusion coefficient distribution $G(D)$ by $D = \Gamma/q^2$. When $x > 1$, the contributions of the internal relaxation processes to $G(\Gamma)$ becomes more and more appreciable, which are not diffusive.

LLS Instrumentation. A commercial LLS spectrometer (ALV/SP-150 equipped with an ALV-5000 multi-τ digital correlator) was used with a solid-state laser (ADLAS DPY425II, output power ≈ 400 mW at $\lambda = 532$ nm) as the light source. The incident beam was vertically polarized with respect to the scattering plane. In our setup, β in eq 5 was ~0.9. With proper modifications,[11] our LLS spectrometer is capable of doing both static and dynamic LLS continuously in a wide angle range of ($6° \le \theta \le 154°$). In static LLS, the precise differential refractive index increment dn/dC at $\lambda = 532$ nm was determined by a differential refractometer designed and constructed in our laboratory.[20] All measurements were done at $T = 15.0 \pm 0.1$ °C. The details of instrumentation and its principles can be found elsewhere.[17]

Results and Discussion

Figure 1 shows typical plots of the line-width distributions $G(\Gamma/q^2)$ of the PNIPAM linear chains (○) and spherical microgel particles (□) at $\theta = 7°$ and $T = 15.0$ °C. As expected, only a single, narrow peak was observed for each case when θ is small. The average line width $\langle\Gamma\rangle$ [$=\int_0^\infty G(\Gamma)\Gamma\,d\Gamma$] is a linear function of q^2 at $x < 1$ and the relaxation is diffusive. Therefore, Γ can be related to the translational diffusion coefficient

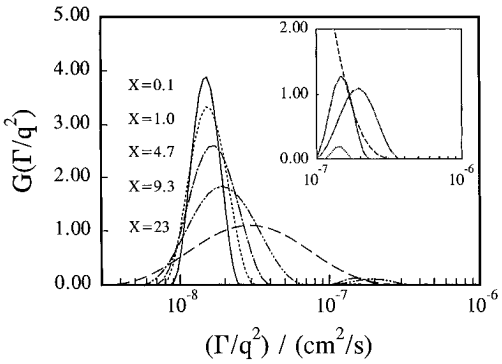

Figure 2. Typical line-width distributions $G(\Gamma/q^2)$ of the PNIPAM linear chains at $T = 15$ °C. The insert shows a tenfold enlargement of the second peak in the range of $10^{-7} < \Gamma/q^2 < 10^{-6}$ cm²/s.

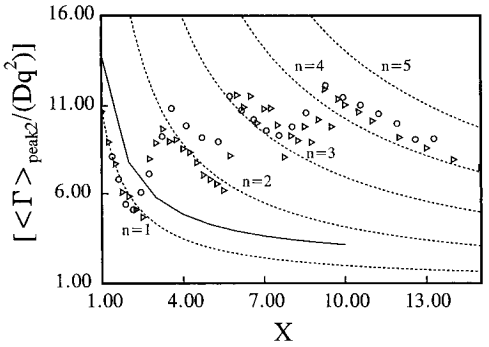

Figure 3. Plots of the reduced average line-width $\Gamma_{peak2}/(Dq^2)$ vs x: (○) PNIPAM linear chains in water at $T = 15$ °C; (△) polystyrene in toluene at $T = 20$ °C (ref 11). The dashed lines are predicted in ref 11, and the full lines are calculated from eqs 7 and 9.

D of the PNIPAM linear chain or spherical microgel particle by $\Gamma = Dq^2$. Further, we can convert D to the hydrodynamic radius R_h by the Stokes−Einstein equation: $R_h = k_B T/(6\pi\eta_0 D)$. D and R_h are also listed in Table 1. The values of R_g/R_h in Table 1 indicate that the PNIPAM linear chains at 15 °C are draining, flexible polymer coils in a good solvent,[21,22] while the swollen PNIPAM microgel networks at 15 °C are nondraining, spherical particles with a uniform density since $R_g/R_h = (3/5)^{1/2} \sim 0.8$ for a uniform hard sphere.

Figure 2 shows typical plots of $G(\Gamma/q^2)$ vs Γ/q^2 for individual PNIPAM linear chains at 15 °C and different x. $G(\Gamma/q^2)$ changes with x. At $x < 1$, there exists only a single narrow peak as discussed before. When $x \sim 1$, a second peak appears at larger Γ/q^2, while the first peak basically retains its position. This second small peak is related to the internal motions of the PNIPAM chain. As x increases further, the first peak becomes broader and shifts to larger Γ/q^2. This is understandable because the observation length scale ($1/q$) is much shorter than R_g at larger x and the observation is well inside the microgel particle. More internal motions with larger Γ contribute to the relaxation and mix with the translational diffusion in the measured spectrum. Finally, two peaks merge into one broader peak because the line width associated with D increases with q, while the line widths related to the internal motions are independent of q.

Figure 3 shows a plot of $\langle\Gamma\rangle_{peak2}/(Dq^2)$ vs x, where $\langle\Gamma\rangle_{peak2}$ is the average line width of the second peak in Figure 2. For comparison, previous experimental data of polystyrene in toluene at 20 °C (ref 11) are also plotted in Figure 3. Clearly, the two plots follow a similar pattern. The dotted lines in Figure 3 show the predicted $[1 + 2\Gamma_n/(Dq^2)]$ dependence on x for polystyrene in toluene.[11] According to existing theories for a flexible polymer coil in the free-draining[23] and nondraining limits,[13] at $x > 1$, $S(q,t)$ depends mainly on the first five relaxation processes, namely, a pure translational term plus four principal internal motions. In decreasing order of the contributions to the spectrum, eq 3 in the time domain at $x > 1$ can be written as

$$S(q,t) = \sum_{n=0}^{\infty} P_n e^{-\Gamma^{(n)}t} \tag{7}$$

where $\Gamma^{(0)} = Dq^2$, $\Gamma^{(1)} = Dq^2(1 + 2\Gamma_1/(Dq^2))$, $\Gamma^{(2)} = Dq^2(1 + \Gamma_2/(Dq^2))$, $\Gamma^{(3)} = Dq^2(1 + 4\Gamma_1/(Dq^2))$, and $\Gamma^{(4)} = Dq^2(1 + 2\Gamma_2/(Dq^2))$; and P_n (the numeric values) in the range of $1 \le x \le 10$ have been calculated by PPC.[13] On the basis of the Zimm model,[2]

$$\Gamma_n = \frac{0.293RT\lambda_n'}{\eta_0 M[\eta]} \tag{8}$$

where $[\eta]$ is the intrinsic viscosity and λ_n' are the eigenvalues in the Zimm model.[24] Using Dq^2 as a unit and replacing q with x, we can rewrite eq 8 as

$$\Gamma_n/(Dq^2) = \frac{0.293\lambda_n' R_g^{\,2} RT}{x^2 M[\eta] D\eta_0} \tag{9}$$

where $RT/(D\eta_0) = 6\pi R_h N_A$ (the Stokes−Einstein equation) so that

$$\Gamma_n/(Dq^2) = \frac{5.52\lambda_n' R_g^{\,2} R_h}{x^2 M[\eta]} = \frac{5.52\lambda_n'(R_g/R_h)^2}{x^2}\frac{R_h^{\,3}}{M[\eta]} \tag{10}$$

where $M[\eta]$ is a measure of hydrodynamic volume, $M[\eta]/R_h^3 = \Phi$ (the Flory constant), which is widely used as the universal calibration in GPC, and R_g/R_h depends weakly on the nature of polymer and solvent for flexible linear polymer chains in a good solvent. Therefore, eq 10 predicts that Γ_n should be independent of polymer and solvent for polymers in good solvents. Figure 3 shows that the two sets of results from completely different polymer/solvent systems folllow a very similar pattern, which indicates that the prediction of eq 10 is essentially correct.

By using the numeric values of P_n in ref 13 and the values of Γ_n calculated from eq 9 for polystyrene in toluene at 20 °C, we were able to calculate the average line width $\langle\Gamma\rangle_{int}$ associated with the internal motions.[11,18] The plot of $\langle\Gamma\rangle_{int}/(Dq^2)$ vs x (the solid line) is shown in Figure 3. If eq 7 was right, $\langle\Gamma\rangle_{peak2}/(Dq^2)$ would follow the solid line. But, Figure 3 shows a clear deviation between the data and the solid line. On the other hand, Figure 3 shows that the experimental data have a tendency to respectively follow the dotted lines of $n = 1$ in $3 < x < 6$; $n = 2$ in $3 < x < 6$; $n = 3$ in $6 < x < 10$; and $n = 4$ in $10 < x < 15$. Thus, by analyzing $\langle\Gamma\rangle_{peak2}/(Dq^2)$ in Figure 3 with an assumption of $\Gamma_{peak2}/(Dq^2) = 1 + 2\Gamma_n/(Dq^2)$, we are able to estimate Γ_1, Γ_2, Γ_3, and Γ_4 in different ranges of x. For $x > 15$, two peaks in Figure 2 merge into a broader peak, which makes it difficult to get a precise $\langle\Gamma\rangle_{peak2}$ value from the spectral distribution $G(\Gamma)$. Therefore, we stopped the second-peak analysis at $x > 15$ to avoid any ambiguity. Polystyrene in toluene and PNIPAM in water show that the internal motions associated with $2\Gamma_n$, i.e., $\Gamma_n + \Gamma_n$, dominate the

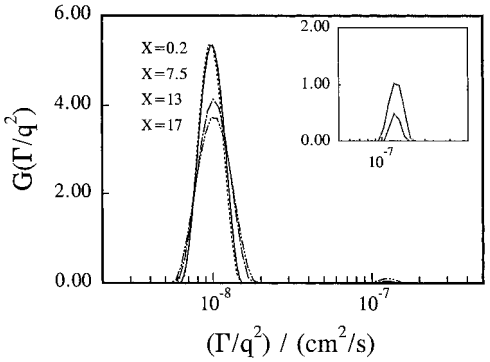

Figure 4. Typical plots of $G(\Gamma/q^2)$ vs Γ/q^2 for the microgel particles at $T = 15$ °C. The insert shows a tenfold enlargement of the second peak at $\Gamma/q^2 \sim 10^{-7}$ cm²/s.

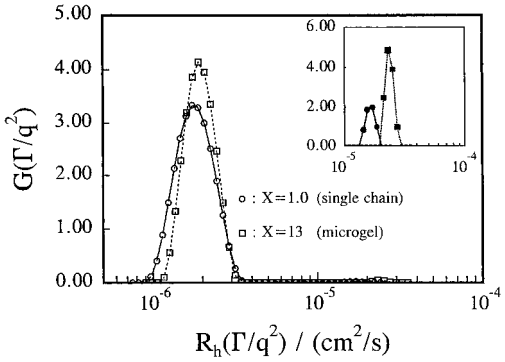

Figure 5. Comparison of $G(\Gamma/q^2)$ of the PNIPAM linear chains at $x \sim 1$ with that of the spherical microgel particles at $x \sim 13$, where the x-axis is shifted by a factor of $R_h(\Gamma/q^2)$, since the PNIPAM linear chains and microgel particles have different hydrodynamic radii.

relaxations measured in dynamic LLS in different ranges of x. On the basis of eqs 3 and 7, this $(\Gamma_n + \Gamma_n)$ relaxation implies a self-coupling of the nth-order internal motion. We have no explanation why only this kind of self-coupled internal motions were observed in dynamic LLS. According to eq 7, energetically, it is easier to excite the internal motions associated with Γ_1 and $4\Gamma_1$ than those associated with $2\Gamma_2$, $2\Gamma_3$, and $2\Gamma_4$. The fact that we observed $2\Gamma_2$ instead of Γ_1 and $4\Gamma_1$ suggests that the ability of dynamic LLS to measure a certain kind of internal motions may be related to the observation length scale, $1/q$. In other words, even though there exist some energetically favorable internal motions, we cannot "see" them in dynamic LLS in a certain range of x. It seems that $P_n(x)$ values in ref 13 have to be modified to take into account the nature of dynamic LLS.

Figure 4 shows plots of $G(\Gamma/q^2)$ vs Γ/q^2 for the spherical PNIPAM microgel particles at 15 °C and different x. $G(\Gamma/q^2)$ is independent of x at $x < 13$ and only a single, narrow peak was observed. When $x > 13$, a very small second peak associated with the internal motions of the microgel network appears. By comparison with Figure 2, we can see that for the linear chains the internal motions start to contribute to $G(\Gamma)$ when $1/q \sim R_g$, while for the particles, the internal motions appear only when $1/q \sim R_g/(13)^{1/2} \sim R_g/3.6$. This tells us that for the linear chain the internal motions involve the entire chain, while for the microgel particle the internal motions are only related to a fraction of the microgel network. The whole microgel particle is not able to undergo a collective volume fluctuation or the internal motions, while a fraction of the network, i.e., a subvolume, can undergo a collective volume fluctuation to show the internal motions.

Figure 5 shows a comparison of the line-width distribution of the PNIPAM linear chains at $x \sim 1$ with that of the spherical microgel particles at $x \sim 13$, where we have used a reduced line width $(R_h\Gamma/q^2)$ for an easier comparison since the linear chains and microgel particles have different hydrodynamic radii. The insert shows a tenfold enlargement of the second peak related to the internal motions. As shown before, if the relaxation is purely diffusive, $R_h\Gamma/q^2$ $[=R_hD = k_BT/(6\pi\eta_0)]$ is a constant for a given temperature and solvent. This is why the two large peaks related to the diffusion of the mass center nearly coincide with each other. Equation 7 and Figure 3 show that at $x \sim 1$, $\Gamma^{(1)}$ $[=Dq^2(1 + 2\Gamma_1/(Dq^2))]$ makes a dominant contribution to $G(\Gamma)$ and $R_h\Gamma^{(1)}/q^2 = R_hD(1 + 2\Gamma_1/(Dq^2))$. On the basis of eq 10, we also know that $\Gamma_1/(Dq^2)$ is independent of polymer and solvent for flexible coils in good solvents. However, the two small peaks (in the insert) related to the internal motions locate at different positions, which is understandable because eqs 7 and 10 are only valid for linear, flexible polymer chains. For a microgel network, the internal motions should involve only a portion of the network. Imaging the portion of the network as an isolated and diffusive one, its diffusion coefficient D^* should be larger than the translational diffusion coefficient D of the whole microgel network. This is why the second peak of the microgel particles is shifted to larger $R_h\Gamma/q^2$ because a lower value of D was used to scale Γ_1. On the other hand, this shift implies that the internal motions inside the microgel network only involve a portion of the network.

At $x \sim 13$, $1/q \sim 44$ nm, which corresponds to the largest linear dimension (radius) of the subvolume involved with the internal motions inside the microgel network. Modeling the network as a three-dimensional lattice, we have estimated that this subvolume contains ~25 lattice units since on average each lattice unit in the swollen state has a linear dimension of ~25 nm.[16] In one dimension, the internal motions involves ~3−4 lattice units, which seems reasonable because each individual subchain between two neighboring cross-links is too short (~25 nm) and too rigid (completely stretched in the swollen state at 15 °C) to display internal motions. It can be imagined that it should be relatively easier for a group of ~25 lattice units to undergo a collective volume fluctuation (internal motions) observed in dynamic LLS. Further experiments are required to verify the size of this estimated subvolume.

Figure 6 shows a plot of $\langle\Gamma\rangle/(q^3k_BT/\eta_0)$ vs $x^{1/2}$ for the PNIPAM linear chains (○) and microgel particles (□) at 15 °C. As x increases, $\langle\Gamma\rangle/(q^3k_BT/\eta_0)$ gradually decreases and approaches a plateau. This scaling of Γ with q^3 is consistent with the nondraining bead-and-spring model for flexible polymer chains in infinitely dilute solution,[25] which was also observed by other laboratories for polystyrene in various organic solvents.[5,10,21] In Figure 6, the plateau value (~0.05) of individual PNIPAM linear chains is close to that of polystyrene in toluene, while the plateau value of the PNIPAM microgel particles is ~3.5 times lower than that of linear polymer chains. As we mentioned before, this much lower plateau value is exactly as expected since the cross-linking has greatly suppressed the internal motions inside the microgel network, while the relaxations associated with the internal motions have larger Γ in comparison with the line width $(\Gamma = Dq^2)$

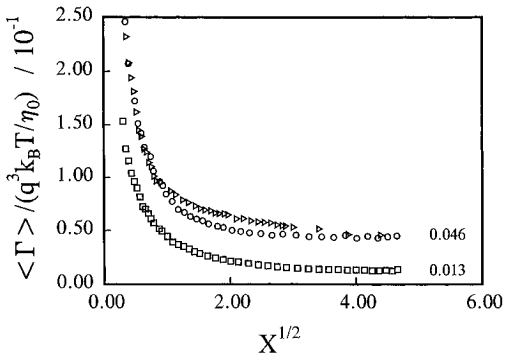

Figure 6. Plots of $\langle\Gamma\rangle/(q^3k_BT/\eta_0)$ vs $x^{1/2}$ for the PNIPAM linear chain (○) and microgel particle (□) at $T = 15$ °C. The previous data (ref 11) of polystyrene in toluene (△) are plotted for comparison.

related to the pure translational diffusion, so that the average line width $\langle\Gamma\rangle$ is lower. We noted before that even for polystyrene in organic solvents, the plateau values are lower than the predicted values,[11] namely, 0.071 and 0.079 with or without a preaveraged Oseen tensor.[5] In this study, the lower plateau value of the PNIPAM linear chain in water supports, but does not prove, the assumption[11] that a number of energetically favorable internal motions are not observable in dynamic LLS at a particular x due to the observation length scale $1/q$.

Acknowledgment. The financial support of the RGC (the Research Grants Council of the Hong Kong Government) Earmarked Grant 1994/95 (CUHK 299/94P, 221600260) is gratefully acknowledged.

References and Notes

(1) Rouse, P. E., Jr. *J. Chem. Phys.* **1953**, *21*, 1272.
(2) Zimm, B. H. *J. Chem. Phys.* **1956**, *24*, 269.
(3) Pecora, R. *J. Chem. Phys.* **1968**, *49*, 1032.
(4) de Gennes, P.-G. *Physics* **1967**, *3*, 37.
(5) Han, C. C.; Akcasu, A. Z. *Macromolecules* **1981**, *14*, 1080.
(6) Chu, B. *J. Polym. Sci., Polym. Symp.* **1985**, *73*, 137.
(7) Kramer, O.; Frederick, J. E. *Macromolecules* **1972**, *5*, 69.
(8) Fujimi, S.; Maruyana, M. *Macromolecules* **1973**, *6*, 237.
(9) Tagami, Y.; Pecora, R. *J. Chem. Phys.* **1969**, *51*, 3293.
(10) Chu, B.; Wang, Z.; Xu, J. *Macromolecules* **1991**, *24*, 6832.
(11) Wu, C.; Chan, K. K.; Xia, K. *Macromolecules* **1995**, *28*, 1032.
(12) Pecora, R. *J. Chem. Phys.* **1965**, *43*, 1762.
(13) Perico, A.; Piaggio, P.; Cuniberti, C. *J. Chem. Phys.* **1975**, *62* (7), 2690; **1975**, *62* (12), 4911.
(14) Zhou, S. Q.; Fan, S. Y.; Au-yeung, S. T. F.; Wu, C. *Polymer* **1995**, *36*, 1341.
(15) Wu, C.; Zhou, S. Q. *Macromolecules*, accepted.
(16) Wu, C.; Zhou, S. Q. *Macromolecules*, submitted.
(17) Chu, B. *Laser Light Scattering*, 2nd ed.; Academic Press: New York, 1991.
(18) Berne, B.; Pecora, R. *Dynamic Light Scattering*; Plenum Press: New York, 1976.
(19) Provencher, S. W. *Biophys. J.* **1976**, *16*, 29; *J. Chem. Phys.* **1976**, *64*, 2772; *Makromol. Chem.* **1979**, *180*, 201.
(20) Chi Wu, Xia, K. Q. *Rev. Sci. Instrum.* **1993**, *65*, 587.
(21) Huber, K.; Bantle, S.; Lutz, P.; Burchard, W. *Macromolecules* **1985**, *18*, 1461.
(22) Akcasu, A. Z.; Han, C. C. *Macromolecules* **1979**, *12*, 276.
(23) Sorlie, S. S.; Pecora, R. *Macromolecules* **1988**, *21*, 1437.
(24) Zimm, B. H.; Roe, G. M. *J. Chem. Phys.* **1956**, *24*, 279.
(25) Dubois-Violette, E.; de Gennes, P.-G. *Physics* **1967**, *3*, 181.

MA950677K